RESEARCH ARTICLE

Check for updates

A recyclable MOF@polymer thin film composite for nanomolar on-site fluorometric detection of heavy metal ion and anti-histamine drug and efficient heterogeneous catalysis of Friedel−Crafts alkylation†

Sk Sakir Hossain,[a] Veerappan Karthik,[b] Amarajothi Dhakshinamoorthy [ID] *[b,c] and Shyam Biswas [ID] *[a]

Developing a robust, reliable, fast-detecting sensor is a significant challenge for present-day researchers. Hence, a dual-functional fluorometric sensor was designed to detect heavy metal ions (*e.g.*, Hg^{2+}) and anti-histamine drugs (*e.g.*, ranitidine) at the nanomolar level in the aqueous medium. A stable and efficient thiourea-functionalized aluminum−based metal-organic framework (MOF) was prepared and its guest-free form was applied for the selective detection of the above-mentioned analytes with a low detection limit (Hg^{2+} = 7.3 nM and ranitidine = 3.4 nM). The MOF was exceptionally sensitive to Hg^{2+} and ranitidine detection with a fast response time of 10 s and 5 s, respectively. Our probe has the highest K_{SV} values for these targeted analytes among the sensors documented to date (*i.e.*, $1.29 \times 10^6 \ M^{-1}$ for Hg^{2+} and $7.99 \times 10^5 \ M^{-1}$ for ranitidine). This work reports the first MOF-based sensor for ranitidine detection. About 93% and 98% fluorescence quenching was observed after introducing Hg^{2+} and ranitidine, respectively. The probe has excellent selectivity toward detecting Hg^{2+} and ranitidine, even in the presence of interfering analytes. The sensing capability of the probe was explored in different media, including serum, urine, wastewater, different pH, *etc.*, which indicates the real-field applicability of the sensor. A cost-effective, highly efficient, long-lasting MOF@polymer thin-film composite (MOF@PVDF-PVP) was employed for the on-field qualitative detection of Hg^{2+} and ranitidine. The mechanistic insights into the sensing were well explored with the help of different modern analytical techniques. The ground-state complexation and inner filter effect were responsible for fluorescence quenching in the presence of Hg^{2+} and ranitidine, respectively. Furthermore, the catalytic performance of **1'** was investigated in the Friedel−Crafts alkylation reaction between indole and β-nitrostyrene in toluene at 70 °C and the product was observed in 98% yield. The solid maintained its activity up to four cycles. The integrity and morphology of the four times used **1'** are identical to those of pristine **1'**. The catalyst was also active to prepare a series of products under the optimized conditions.

[a] *Department of Chemistry, Indian Institute of Technology Guwahati, Guwahati, 781039 Assam, India. E-mail: sbiswas@iitg.ac.in*
[b] *School of Chemistry, Madurai Kamaraj University, Madurai-625 021, Tamil Nadu, India. E-mail: admguru@gmail.com*
[c] *Departamento de Química, Universitat Politècnica de València, C/Camino de Vera, s/n, 46022, Valencia, Spain*

† Electronic supplementary information (ESI) available: Linker synthesis details, ^{1}H NMR, mass, and ^{13}C NMR spectra of free linker, ATR-IR spectra of MOF and free linker, TGA plot, EDX spectrum, BET isotherms, fluorescence spectra, TRPL plot, UV-vis spectra, recyclability plot, and catalytic data. See DOI: https://doi.org/10.1039/d3qi01890c

Introduction

The toxicity of mercury has been recognized for centuries with historical records describing its harmful effects on miners and artisans exposed to fumes and vapors.[1] The toxicity of mercury was further highlighted in the late 19th century when Minamata disease, a neurological disorder caused by consuming fish contaminated with mercury, was reported in Japan.[2] Research on the mechanisms of mercury toxicity has shown that it can bind to proteins and enzymes, disrupting their function and leading to cell damage and death.[3] It can also cross the blood–brain barrier, leading to neurological damage and cognitive impairment.[4] Moreover, mercury can accumulate

in the body over time, leading to chronic exposure and increased risk of toxicity. The US-EPA has established strict concentration limits for mercury in water, set at 2 parts per billion (ppb).[5] Overall, the history of mercury toxicity highlights the importance of understanding the risks involved during contact to this toxic metal and the need for monitoring and controlling its levels in the environment to protect human health and the ecosystem.

Ranitidine is a widely used medication belonging to histamine-2 receptor antagonists. It is commonly prescribed to individuals suffering from gastrointestinal disorders, such as acid reflux, peptic ulcers, and heartburn.[6] The primary function of ranitidine is to alleviate these conditions by reducing the production of stomach acid. Ranitidine sensing in different biological media (plasma and serum) is vital for therapeutic drug monitoring. By measuring the levels of ranitidine in a patient's blood or plasma, healthcare professionals can determine the drug's concentration and ensure that it falls within the optimal therapeutic range. This information allows for dosage adjustments, ensuring patients receive the appropriate medication to manage their gastrointestinal condition effectively.

Ranitidine can have adverse effects on the environment. It can enter water bodies through sewage systems and wastewater treatment plants, causing aquatic toxicity and disrupting the growth and survival of aquatic organisms. Ranitidine also has the potential to bioaccumulate in organisms, leading to higher concentrations in predators. Its improper disposal or presence in wastewater can contaminate groundwater, posing risks to drinking water sources. Additionally, the use of ranitidine has been associated with the development of antimicrobial resistance.[7] Proper management and disposal practices are essential to mitigate the environmental impact of ranitidine.

In aqueous media, detecting Hg^{2+} ions has been challenging due to the interference from other metal ions and the low concentration of Hg^{2+} ions. Similarly, detecting ranitidine in biological medium is also quite difficult due to other components in a complex medium. Several techniques have been introduced for detecting these analytes, including chromatography,[8] electrochemical,[9] and fluorometric[1] based sensing. Among these methods, the fluorescence-based method is one of the most popular techniques due to its simple and easy handling processes.[10] Different fluorescent probes have been designed to detect Hg^{2+} ions and ranitidine, including organic molecular probes, quantum dots, carbon nanotubes, and MOFs.[11–14] Among them, MOFs are potential materials for sensing applications owing to their high surface area, tunable pore sizes, and easily functionalized structures.[15,16]

After going through several reported works, we found that sulfur-containing fluorophores could respond to the presence of Hg^{2+} ions, following the HSAB principle. We observed the UV-vis absorption maximum of ranitidine at 325 nm. Hence, a probe with an excitation maximum near 325 nm could detect ranitidine through a non-radiative energy transfer pathway. This idea was explored by synthesizing a thioureido containing fluorophore-based Al-MOF (Scheme 1). Our probe can detect
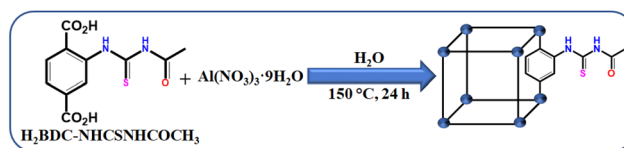
Scheme 1 Schematic diagram for the synthesis of **1**.

Hg^{2+} and ranitidine in aqueous and HEPES buffer (pH = 7.4) media. The fluorescence quenching efficiencies of Hg^{2+} and ranitidine were 93% and 98%, respectively. Different modern analytical techniques were employed to investigate the mechanism of sensing thoroughly. The sensing ability of the probe towards the targeted analytes was explored in different real water samples and in different pH media. A polyvinylidene difluoride-polyvinylpyrrolidone (PVDF-PVP) thin film-based MOF composite was also introduced for qualitative point-of-care detection of these analytes. The real-field applicability, selectivity, and ultralow detection limit make our designed probe distinct for detecting Hg^{2+} and ranitidine.

The Friedel–Crafts alkylation reaction between β-nitrostyrene (NS) and indole (IND) is one of the reactions often employed as a prototypical reaction to screen the catalytic activity of MOF solids.[17–20] Besides, this reaction can also be considered as a straightforward reaction to access a series of heterocyclic compounds exhibiting a wide range of biological activities. In addition, this reaction is also used by many researchers to demonstrate the influence of different functionalities embedded within the framework and to establish size-selective catalysis.[21] The Friedel–Crafts alkylation reaction between IND and NS has been reported by using a series of MOFs that include CSMCRI-17,[22] La(III)-MOF,[23] urea-modified MOFs,[24] urea-modified UiO-67,[25] UiO-66(Ce),[26] amide functionalized MOFs,[27] $Cu_3(BTC)_2$[28] and squaramide functionalized Zr-MOF.[29] Thus, the present work aims to address the influence of the thioureido functionality on Al-based MOFs as well as size-selective catalytic behavior. Beside these primary objectives, catalyst stability and substrate scope were also investigated.

Experimental section

Synthesis of [Al(OH)(BDC–NHCSNHCOCH₃)]·H₂O (1)

The detail of linker synthesis is mentioned in the ESI.† The MOF was synthesized using a conventional solvothermal approach. The optimized conditions for the MOF synthesis were obtained by varying the aluminium salts, solvents (such as H_2O, DMF and their mixtures) and temperature (starting from 100 to 180 °C). The optimized conditions for MOF synthesis are as follows: in a 100 mL Teflon-lined autoclave, 216 mg (0.57 mmol) of $Al(NO_3)_3 \cdot 9H_2O$, 160 mg (0.57 mmol) of 2-(3-acetylthioureido)terephthalic acid (H₂BDC–NHCSNHCOCH₃) and 10 mL water were placed (Scheme 1). The Teflon vial was sonicated for 30 minutes and then put in an autoclave. Finally, the Teflon-lined autoclave was kept in a preheated oven at 150 °C for one day. It was naturally cooled to

room temperature after one day. A slightly yellowish precipitate was acquired after filtration. The solid was washed thoroughly with water, DMF and acetone to remove the unreacted starting materials. Finally, the obtained product was dried overnight at 80 °C in a hot air oven. Yield: 131 mg (0.38 mmol, 67%) with respect to the Al-metal salt.

Activation of the as-synthesized MOF (1)

The activation of the MOF was executed by the following way. At first, the as-synthesized MOF **1** (30 mg) was suspended in 30 mL MeOH and the suspension was stirred at room temperature for 24 h. After that the suspension was filtered out, washed several times with MeOH and finally dried in an oven overnight at 120 °C. The MOF was heated under vacuum at 100 °C to get the activated MOF. All the sensing experiments were performed using the activated MOF (**1′**).

Preparation of the 1′@PVDF-PVP thin film composite

The MOF-based thin-film composite was prepared by adopting a method previously reported in the literature with some modifications.[30] Typically, 200 mg of PVDF and 50 mg of PVP were mixed with 3 mL of DMF and kept under stirring for 2 h. After that, 10 mg of **1′** was added and stirred for 6 h. Then, 500 μL of the obtained suspension was placed on a glass slide with spin coating at 800 rpm for 40 s. Finally, the glass slide was kept at 75 °C in an oven for 2 h to obtain the **1′@PVDF-PVP** thin-film composite.

Results and discussion

Structural interpretation

MIL-53(Al) is a type of MOF with a porous structure composed of BDC ligands and Al^{3+} ions.[31] The framework consists of $[AlO_4(OH)_2]$ octahedral clusters. These clusters form a linear chain by connecting through μ_2-OH bridging. These chains are linked together by carboxylate groups from four different BDC ligands to generate a three-dimensional framework. The framework contains large one-dimensional rhombic shaped channels that run parallel to each other. The functionalization of the BDC ligand usually does not influence the structure of the MOF. Inspired from this observation, we synthesized an aluminium MOF functionalized with the $-NHCSNHCOCH_3$ group in the BDC ligand.

The sharp peaks in the PXRD profile of **1** revealed the high crystallinity of the synthesized MOF material. The PXRD patterns of **1** and **1′** are almost similar to that of the parent MOF (Fig. 1b). These findings confirm the high structural similarity of **1** with the parent MOF. This structural similarity was further supported by Pawley refinement of PXRD profile of **1′**
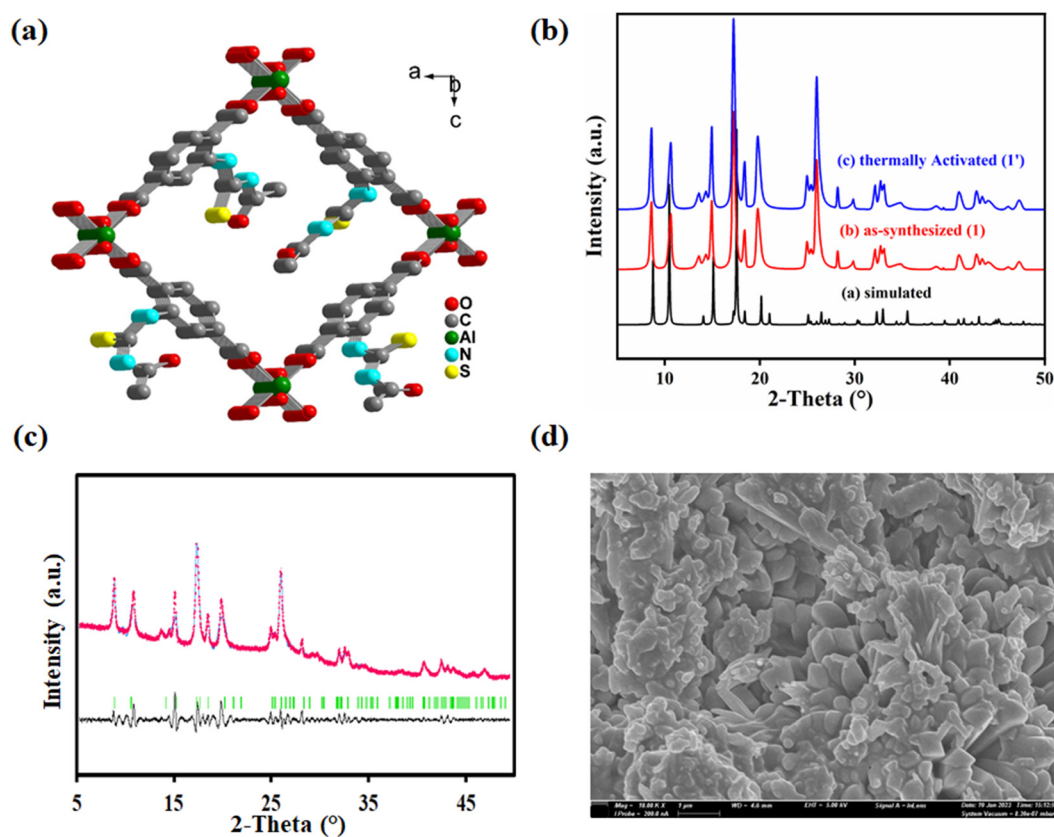

Fig. 1 (a) Simulated structure of **1**. (b) PXRD profiles of **1** and **1′** compared with simulated one. (c) Pawley refinement plot for the slow scan PXRD profile of **1′** (R_{wp} and R_p are 5.4% and 3.8%, respectively). (d) FE–SEM image **1′**.

(Fig. 1c). The obtained lower values R_p = 5.3% and R_{wp} = 3.4% suggest the high similarity between the observed and simulated PXRD profiles of **1′**.

The FE-SEM images were collected to investigate the morphology of the synthesized MOF. A homogeneous distribution of nano-rod shaped particles was observed in the FE-SEM images of **1′**, a common morphology of the pristine MOF (Fig. 1d). The average diameter of the particles, observed from DLS measurement, was 589 nm (Fig. S3†). Apart from these findings, the EDX spectrum (Fig. S4†) of **1′** was also recorded to confirm the presence of the desired elements *i.e.* C, O, N, S and Al in the MOF. The EDX elemental mapping (Fig. S5†) signified the homogeneous distribution of the above elements in **1′**.

Functional group analysis

It was previously reported that the carbonyl stretching frequency of the carboxylic acid linker is shifted to lower wavenumbers when it is co-ordinated to metal ions.[32] We performed ATR-IR experiment to validate the above statement in our case. The results (Fig. S6†) show that the $-C{=}O$ stretching frequency for carboxylate is observed at 1595 cm^{-1} in **1** and **1′**, whereas the same for the linker is noticed at 1643 cm^{-1}. Another common peak is observed at 1705 cm^{-1} for the linker, **1** and **1′**, which verifies the presence of the amide functionality and supports the intact nature of the desired functionality in the synthesized MOF. Apart from these peaks, a peak at around 1204 cm^{-1} suggests the existence of the $-C{=}S$ functional group appended with the linker molecule. Moreover, the ^{1}H NMR spectrum (Fig. S7†) of digested **1′** revealed the retention of the desired functionality in the synthesized MOF.

Chemical and thermal stability of 1′

A sensor should be stable in different chemical environments, most importantly in the sensing medium. We executed the PXRD analysis of **1′** after stirring in various solvent media such as water, HEPES buffer, different pH media, and commonly used organic solvents. The results confirmed the high chemical stability of **1′** under these conditions (Fig. S8†).

The TG analysis of **1** and **1′** was conducted under N_2 atmosphere to determine their thermal stability (Fig. S9†). For compound **1**, a weight loss of 4.9% was observed in the 30–300 °C temperature range due to the loss of one water molecule per unit formula of **1** (calculated weight loss was 4.9%). After 300 °C, a continuous weight loss was observed, which implies the breaking of the framework. A similar weight loss step was followed for **1′**, except for the weight loss due to the elimination of water molecules. Hence, both the samples were stable up to 300 °C.

Overall, the results from PXRD and TG analyses highlight the high chemical and thermal stabilities of **1′** in diverse chemical environments, making it a promising sensor for various applications.

N₂ sorption study

One of the most intriguing properties of a MOF is its porous nature. We performed N_2 sorption analysis of **1′** at −196 °C in order to determine its surface area. The obtained result is depicted in Fig. S10.† The surface area of **1′** was found to be 146 m^2 g^{-1}, which is much lower than that of the un-functionalized MOF. It was previously reported that the surface area of MOF is reduced drastically upon functionalization because the functional groups occupy the cavity of the MOF and reduce its surface area.[33] Therefore, our result is consistent with the reported results.

Fluorometric sensing of Hg²⁺ and ranitidine in water

We have chosen water as a medium for sensing of Hg^{2+}. Hence, we prepared the MOF suspension in water. The details of the preparation of the MOF suspension are described in the ESI.† All the fluorescence measurements were performed with this aqueous MOF suspension. The excitation and emission spectra of the MOF suspension in water and HEPES buffer are presented in Fig. S11 and S12.† We have also recorded the excitation and emission spectra of the ligand (Fig. S13†). The fluorometric titration experiment for Hg^{2+} detection was executed using 3 mL of water and 100 µL of MOF suspension, followed by the addition of 10 mM analyte solution to it. A similar protocol was used for the detection of ranitidine with some modifications. In this case, both the preparation of MOF suspension and the sensing experiment were performed in HEPES buffer (pH = 7.4) medium and 5 mM analyte solution was used for fluorometric titration experiments. The rest of the fluorescence titration experiments were like those for Hg^{2+} recognition. The MOF suspension was excited at 322 nm for all the sensing experiments and the emission spectra were collected in the range of 342–550 nm.

A systematic volume-dependent fluorescence sensing experiment was executed to determine the volume of 10 mM Hg^{2+} solution required for the maximum possible fluorescence quenching. This experiment was performed upon the incremental addition of 25 µL of 10 mM Hg^{2+} solution to the aqueous MOF suspension (3100 µL). Upon gradual addition of Hg^{2+} solution, the fluorescence emission intensity of the probe showed gradual reduction, as depicted in Fig. 2a. There was no further fluorescence quenching after the addition of 100 µL of Hg^{2+} solution (10 mM concentration).

In a similar way, the volume-dependent fluorometric titration experiment was executed for ranitidine sensing in HEPES buffer medium with incremental (50 µL for each step) addition of 5 mM ranitidine solution. For ranitidine recognition, the maximum fluorescence quenching occurred after the addition of 200 µL of 5 mM ranitidine solution, as depicted in Fig. 2b. The quenching efficiency for both analytes were calculated using the formula $(1 - I/I_0) \times 100$, where I_0 and I represent the fluorescence intensity of **1′** before and after the addition of the targeted analyte, respectively. It was found that the probe's 93% and 98% fluorescence intensity was quenched after introducing 100 µL and 200 µL of 10 mM Hg^{2+} and 5 mM ranitidine solution, respectively.

We also conducted the time-dependent fluorescence titration experiment in order to determine the response time of our synthesized probe **1′**. For time-dependent fluorescence
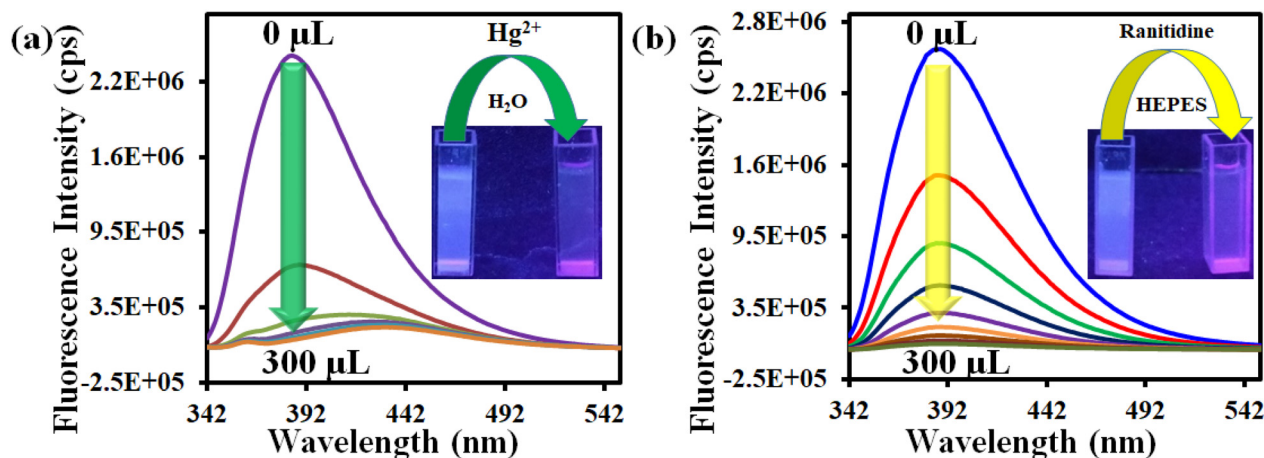
Fig. 2 Change in the fluorescence intensity of **1'** after incremental addition of (a) 10 mM Hg^{2+} and (b) 5 mM ranitidine solutions in aqueous and HEPES buffer media, respectively.

titration experiment, 100 μL of 10 mM Hg^{2+} solution was added at a time to 3100 μL MOF suspension. The fluorescence data were recorded with a time interval of 5 s. There was 93%

fluorescence quenching of the probe within 10 s after introducing 100 μL of 10 mM Hg^{2+} solution and no further quenching was observed after 10 s (Fig. 3a). This was confirmed by per-
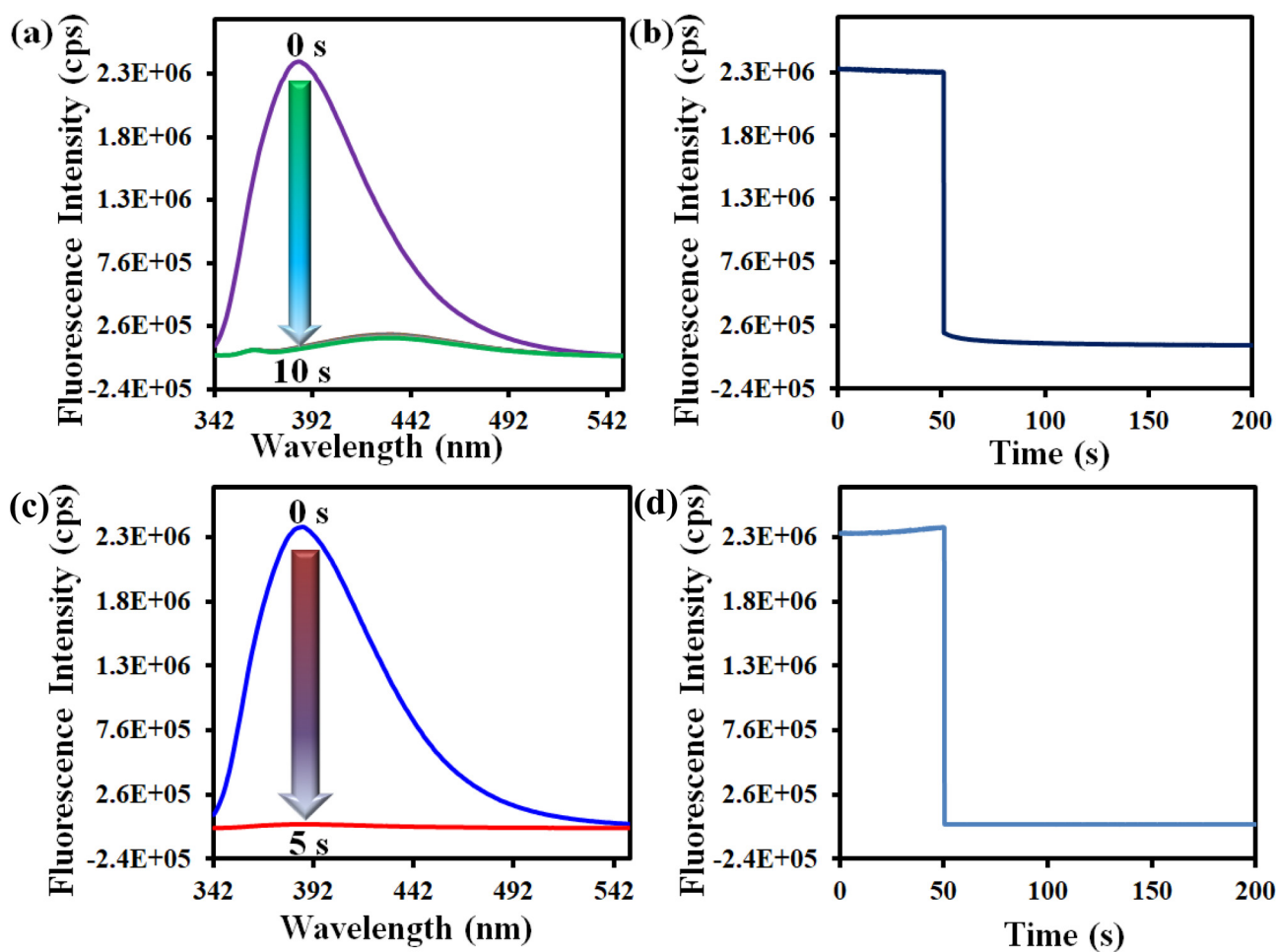
Fig. 3 Time-dependent variation in the fluorescence spectra of **1'** after addition of (a) 100 μL of 10 mM Hg^{2+} and (c) 200 μL of 5 mM ranitidine solution in aqueous and HEPES buffer media, respectively. Results of fluorescence kinetic experiments for (b) Hg^{2+} and (d) ranitidine.

forming kinetic experiment. In fluorescence kinetic experiment, the fluorescence intensity of the MOF at 388 nm was recorded with respect to time (up to 50 s) upon excitation at 320 nm. After 50 s, we added 100 µL of 10 mM Hg^{2+} solution and recorded the fluorescence intensity for up to 200 s. The result shows that 93% quenching took place within 10 s (Fig. 3b). Similar protocols were adopted to determine the response time of 1′ toward ranitidine sensing. It was observed that the fluorescence intensity was quenched by 98% within 5 s upon introduction of 200 µL of 5 mM ranitidine solution (Fig. 3c and d). Therefore, it can be concluded that our probe has ultrafast detection time for both the analytes in comparison to other fluorescent sensors reported to date (Table S7†).

An ideal sensor should respond to a target analyte in the presence of other interfering analytes. In this regard, the selectivity of 1′ towards Hg^{2+} was investigated in the presence of different metal ions like Cu^{2+}, Ag$^+$, K$^+$, Na$^+$, Cd^{2+}, Zn^{2+}, Mg^{2+}, Mn^{2+}, Pb^{2+}, Ni^{2+}, Fe^{2+}, Pt^{2+}, Pd^{2+}, Al^{3+}, Cr^{3+} and Co^{2+}. We have used different counter anions for different metal ions (Cl$^-$, SO$_4^{2-}$, NO$_3^-$, NO$_2^-$, F$^-$, CH$_3$COO$^-$, etc.). The interference study was also conducted by using the sodium salts of these counter anions (Fig. S14–S37†). To examine the selectivity towards Hg^{2+}, 100 µL of each competitive analyte solution (10 mM concentration) was added to the probe suspension. Subsequently, 100 µL of 10 mM Hg^{2+} solution was added. As

depicted in Fig. 4a, no analyte had a quenching efficiency more than 30%, except Hg^{2+} which showed a quenching efficiency of 93%. Moreover, the interfering analytes did not alter the quenching efficiency of the probe considerably (Fig. 4c).

In order to examine the selectivity towards ranitidine, 200 µL solution of individual competitive analyte solution (5 mM concentration) was added to the dispersion of the MOF and subsequently 200 µL of 5 mM ranitidine solution was added. The competitive analytes of ranitidine included glucose, alanine, phenylalanine, histidine, K$^+$, Na$^+$, Mg^{2+}, aspartic acid, glutamic acid, serine, tartaric acid, ascorbic acid, creatinine, glutathione, uric acid and urea (Fig. S38–S53†). As depicted in Fig. 4b, all the analytes showed less than 25% quenching efficiency except for ranitidine, which exhibited a quenching efficiency of 98%. Furthermore, the quenching efficiency of ranitidine was not hampered by the presence of different analytes (Fig. 4b–d).

Stern–Volmer constant (K_{SV}) is directly related to the quenching efficiency of a quencher. A higher value of K_{SV} signifies higher quenching and vice versa. We plotted I_0/I as a function of analyte concentration for both Hg^{2+} and ranitidine to evaluate the K_{SV} values for both the targeted analytes (Fig. S54 and S55†). The obtained K_{SV} values are 1.29×10^6 M^{-1} and 7.99×10^5 M^{-1} for Hg^{2+} and ranitidine, respectively.
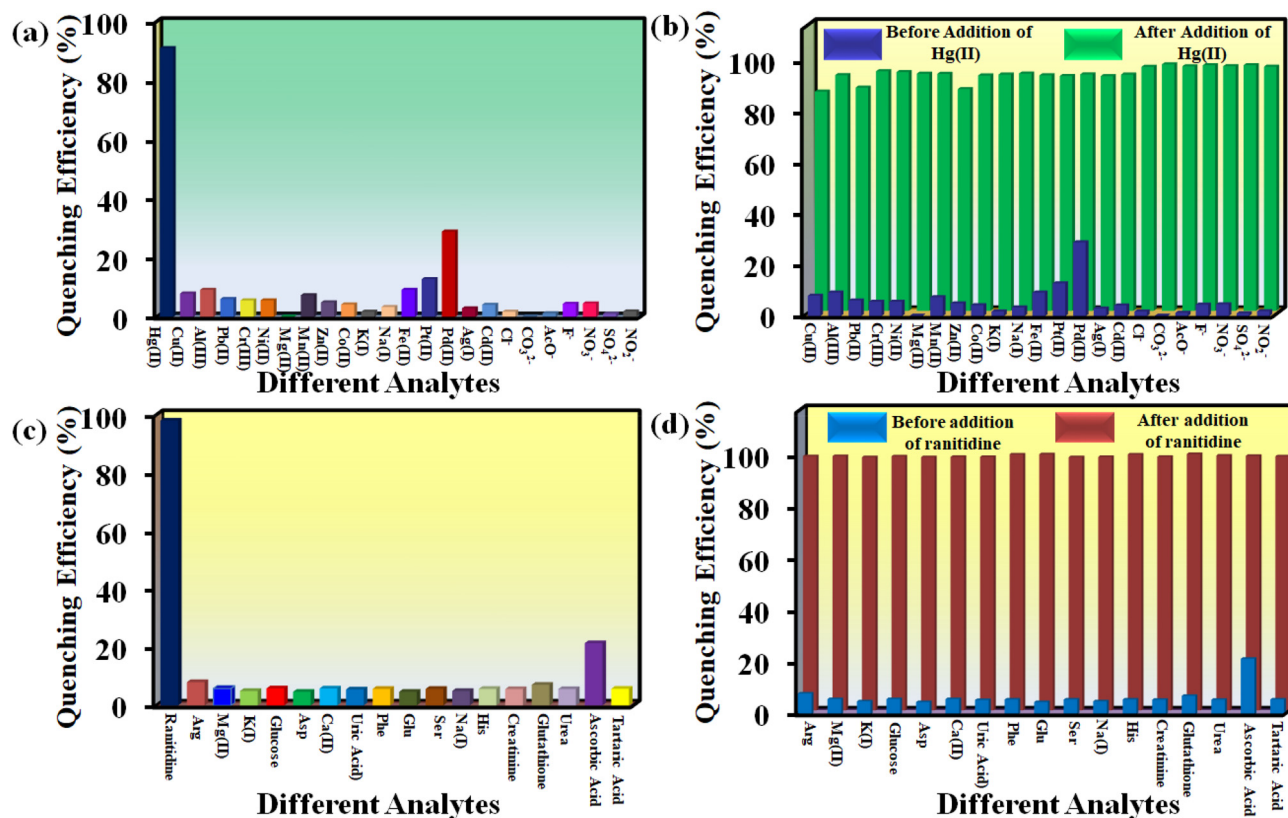

Fig. 4 Selectivity of 1′ towards (a) Hg^{2+} and (c) ranitidine over other analytes and selectivity of 1′ towards (b) Hg^{2+} and (d) ranitidine in presence of other analytes.
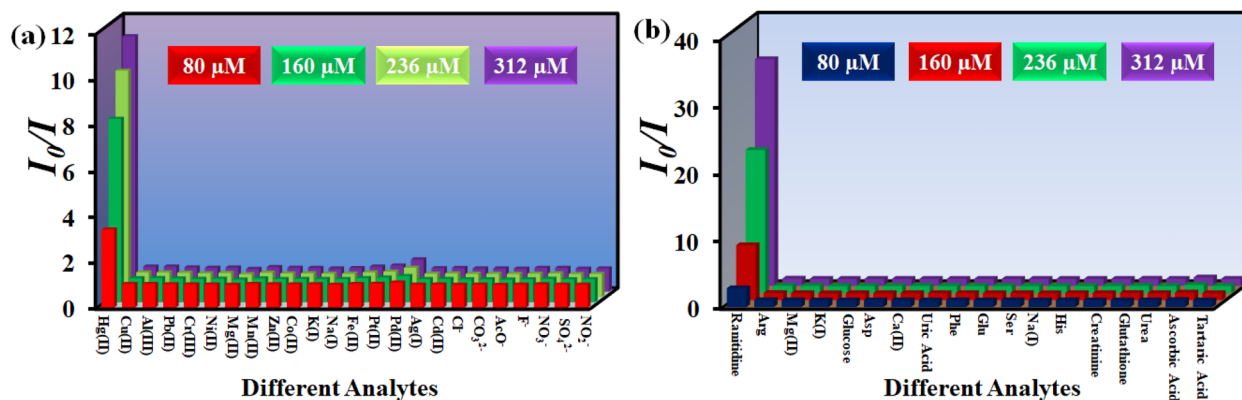
Fig. 5 3D S-V plots of various analytes for (a) Hg^{2+} and (b) ranitidine sensing using **1′**.

These values are higher than those of reported sensors for fluorometric detection of both analytes (Table S7†). From the large values of K_{SV}, it can be inferred that both Hg^{2+} and ranitidine exert strong interactions with the probe. The 3D Stern–Volmer plots of both the targeted analytes are also shown in Fig. 5a and b, which imply that our sensor is highly selective to the targeted analytes in the respective medium.

An ideal sensor should be able to detect very low concentration of an analyte. To estimate our sensor's limit of detection (LOD), we performed fluorescence experiments for both analytes in concentration ranges as low as possible. The formula $3\sigma/k$ was utilized to find out the LOD values for both analytes, where k is slope of the linearly fitted plot of the fluorescence intensity of **1′** *versus* the concentration of analytes (Fig. S56 and S57†) and σ is standard deviation of 10 blank fluorescence readings of MOF suspension. The LOD values are 7.3 nM and 3.4 nM for Hg^{2+} and ranitidine, respectively. The LOD value for Hg^{2+} is comparable to those of previously reported MOF-based sensors (Table S7†). As per our knowledge, this is the first MOF-based ranitidine sensor. The LOD for ranitidine is the lowest amongst the fluorescent sensors reported to date (Table S8†).

Hg^{2+} and ranitidine detection in different water and pH media

Hg^{2+} detection in different water samples (Milli-Q water, river water, tap water and lake water) was investigated systematically. At first, MOF suspensions were prepared in different types of water specimens. Then, we prepared a series of aqueous Hg^{2+} solutions with 1, 2.5 and 5 mM concentrations for our fluorescence sensing experiments. The fluorescence intensity of **1′** in different water specimens was measured before and after the addition of 100 μL solution of different concentrations of Hg^{2+}. The outcomes in terms of quenching efficiency are displayed in Fig. 6a. The results confirmed that our probe is highly effective in detecting Hg^{2+} even from complicated aqueous systems. Similarly, we explored the quenching efficiency of the probe toward Hg^{2+} in different pH media. Our designed probe can detect Hg^{2+} in a broad pH range (4 to 10) without losing its quenching efficiency significantly (Fig. 6b).

Our probe can detect ranitidine in HEPES buffer medium, different water specimens and a wide pH range. The ranitidine

sensing ability of **1′** in various media was investigated in a previously mentioned way as for Hg^{2+}. The obtained results are depicted in Fig. 6c and d. These findings suggest that our probe can be used for real-field monitoring of Hg^{2+} and ranitidine.

Detection of ranitidine in human urine and blood serum

The fluorometric detection of ranitidine was also performed in more complicated environments like urine and human blood serum. The procedures for preparing urine and blood serum samples are provided in the ESI.† A specific amount of ranitidine was added in different serum and urine samples. After that, these solutions were spiked in **1′** and the fluorescence data were recorded. Each experiment was repeated three times to evaluate the measurements' relative standard deviation (RSD). The obtained experimental results are displayed in Fig. S58, S59 and Tables S1, S2.† In both urine and blood serum, the recovery percentages are between 97.0 and 104.0%, and the relative standard deviations are also quite low (0.8 to 3.1%). These findings imply that our probe could be suitable to detect ranitidine even in complex media.

Detection of ranitidine in pharmaceutical samples

Apart from sensing of ranitidine in blood serum and urine samples, we also explored the detection of ranitidine in pharmaceutical compositions such as ranitidine tablets. A ranitidine tablet RANRAC®150 was purchased from a local medical shop (Guwahati, India). One tablet was crushed into powder and 9 mg from it was added in 4 mL HEPES buffer solution. The solution was sonicated to make a homogeneous solution. Then, the centrifugation of the solution was performed at 10 000 rpm for 10 min. The obtained supernatant was used for fluorescence experiments. The experimental results (Fig. S60†) imply that our probe can detect ranitidine even in pharmaceutical samples.

Reusability of **1′**

An ideal fluorescent turn-off sensor should be reusable without losing its quenching efficiency. We studied the recyclability of **1′** for both the analytes for up to five cycles by collect-

148 | *Inorg. Chem. Front.*, 2024, **11**, 142–155
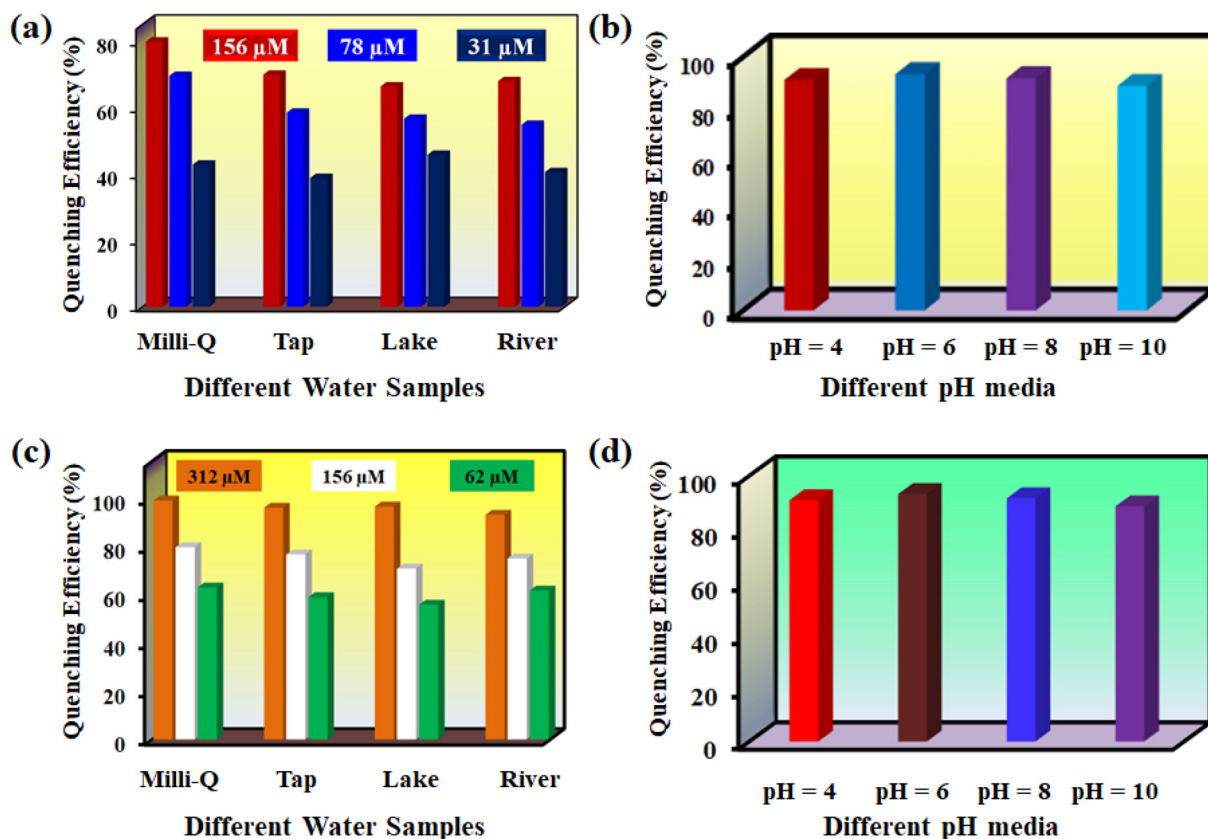
This journal is © the Partner Organisations 2024

Fig. 6 Fluorescence quenching efficiency of (a) Hg^{2+} and (c) ranitidine in different real water specimens and sensing ability of **1′** in different pH media for (b) Hg^{2+} and (d) ranitidine.

ing through centrifugation and washing with a large excess of water after every cycle of sensing in order to remove the analytes. The obtained MOF sample after centrifugation and washing was used for next fluorescence detection cycle. The results showed that **1′** is almost equally efficient up to 5th cycle for sensing of both the targeted analytes in the respective medium (Fig. S61 and S62†). We also examined the stability of **1′** before and after sensing by comparing the PXRD patterns. We found our probe highly stable after sensing both analytes in the respective medium (Fig. S63†).

Sensing of Hg^{2+} and ranitidine with the 1′@PVDF-PVP thin film composite

Excellent selectivity, recyclability and high sensitivity motivated us to introduce an inexpensive user-friendly MOF@PVDF-PVP composite membrane for real-field sensing application of Hg^{2+} and ranitidine. Probe-coated paper strips and cotton-based composites were introduced previously for detection of targeted analytes.[34,35] But, these kinds of composites have several limitations, including leaching of MOF particles, non-reusability, instability in solvents, *etc*. These shortcomings could be overcome by introducing relatively more stable MOF@polymer composite thin film that strongly holds the MOF particles. The thin-film preparation method has been mentioned previously in the Experimental section. The PXRD

patterns and ATR-IR spectra revealed that the MOF particles were grafted on the polymeric surface of the membrane (Fig. S64 and S65†). We found that the thin-film was amorphous in nature. Hence, all the peaks of **1′** could not be assigned to **1′@ PVDF-PVP** but the major peaks of **1′** could easily be assigned. After successfully preparing and characterizing the **1′@PVDF-PVP** membrane, it was treated with different concentrations of analyte solutions. Fig. 7 reveals the decrease in the fluorescence intensities of the composite upon an increase in the concentration of analytes solutions. These observations indicate that the membrane composite could be useful for the real-field monitoring of the targeted analytes.

Mechanism of fluorometric sensing

The mechanism of fluorescence quenching was systematically investigated for both analytes. Our first observation was that probe **1′** showed turn-off responses towards both analytes. According to various reported works, several phenomena might cause the fluorescence quenching, including breaking of the MOF structure, ground-state complexation, the inner filter effect (IFE), Förster resonance energy transfer (FRET), photoinduced electron transfer (PET), *etc*.[10,36–38]

    The obtained PXRD patterns of **1′** (Fig. S63†) before and after detection experiments were analogous, implying the retention of the structural integrity of **1′** after sensing. Then,
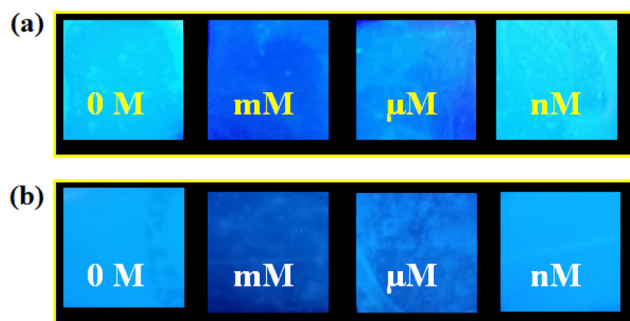
Fig. 7 Detection of various concentrations of (a) Hg^{2+} and (b) ranitidine using the MOF@PVDF-PVP thin film composite.

we executed the time-resolved photoluminescence (TRPL) experiment of **1′** before and after the addition of targeted analytes to evaluate the excited-state fluorescence lifetime of **1′**. The experimental results are displayed in Fig. S66 and S67, and Tables S3 and S4.† It was observed that there were no significant changes in the lifetime of **1′** in the presence of targeted analytes. These results omitted the possibility of PET or FRET-based quenching.

In the case of ground-state complexation, there should be a change in the position of maximum absorbance (λ_{max}) after the addition of analyte, whereas this is unaltered for IFE-based quenching.[37] We observed that the addition of Hg^{2+} to the aqueous suspension of **1′** caused a significant change in the λ_{max} value (Fig. S68†). However, no such variation in the λ_{max} value happened in the case of ranitidine. Ground-state complexation is the most probable reason behind Hg^{2+} sensing as **1′** contains a soft donor S atom and Hg^{2+} is a soft acceptor. We have performed various experiments to establish the feasibility of ground-state complexation between Hg^{2+} and S atoms, including EDX, fluorescence, UV-vis spectrophotometry, isothermal titration calorimetry (ITC), XPS analysis, *etc.*

The EDX spectrum and elemental mapping (Fig. S69 and S70†) of **1′** after treating with Hg^{2+} (without washing) confirmed the presence of Hg^{2+}. The reusability of our probe (Fig. S61†) after thoroughly washing with water implies the presence of weak interaction between Hg^{2+} and **1′**. There was a significant change in both the excitation and emission spectra of **1′** upon introducing Hg^{2+} (Fig. S68†). We have also executed solid-state UV-vis spectroscopy of **1′** before and after treating with Hg^{2+} (Fig. S71†). We found a red shift (32 nm) in the UV-vis spectrum of **1′** after Hg^{2+} addition. These results indicate the formation of a complex between **1′** and Hg^{2+}.

A systematic ITC experiment was performed to further investigate the mechanism of sensing. Various thermodynamic parameters such as binding constant (Ki), enthalpy change (ΔH) and entropy change (ΔS), *etc.*, could be obtained from this experiment. In this experiment, Hg^{2+} solution was used as the titrant while the linker solution was used as the titrate. Both of them were taken in water. A certain amount of Hg^{2+} solution was injected into the linker solution with a constant time interval and the heat change was recorded upon each

injection. The obtained results are depicted in Fig. S72 and Table S5.† The negative values of ΔH and ΔS confirmed that the exothermic complexation reaction occurred after adding Hg^{2+} to the linker solution. These observations again support our mechanistic assumption.

The soft–soft interaction between the 'S' atom and 'Hg^{2+}' was further proved by XPS analysis. The 2s orbital binding energies of sulphur shifted significantly to higher energy after introducing Hg^{2+} in **1′** (Fig. S73†). Apart from this, the shifting of binding energies for all elements was observed before and after the addition of Hg^{2+} (Fig. S74–S78†). These shifts imply the electron transfer from **1′** to Hg^{2+} and the fluorescence quenching of **1′** resulted from it.

In the case of ranitidine, there was no change in lifetime after the addition of ranitidine (Fig. S67 and Table S4†). This result omitted the possibility of dynamic quenching: either FRET or PET. No considerable overlap between the emission spectrum of **1′** and the absorption spectrum of ranitidine (Fig. S79†) excluded the probability of the FRET mechanism.

The possibility of PET behind fluorescence quenching was further investigated by comparing the lowest unoccupied molecular orbital (LUMO) and the highest occupied molecular orbital (HOMO) energies of the free linker and ranitidine. Density functional theory (DFT) was utilized to obtain the HOMO–LUMO of the free linker and ranitidine. All calculations were performed using the Pople diffuse basis set 6-31G+(d, p) and B3LYP functional. The LUMO of the linker has much lower energy than that of ranitidine (Fig. S80†). Therefore, the probability of electron transfer from the excited state of the linker to the LUMO of ranitidine was negligible, which diminishes the possibility of PET behind the detection of ranitidine.

A large overlap was noticed between the excitation spectrum of **1′** and the absorption spectrum of ranitidine (Fig. S79†). This observation suggested that the IFE might be a probable reason behind the fluorescence quenching of the MOF after ranitidine inclusion. We performed UV-vis spectroscopy of the targeted analyte along with all the interfering analytes to prove it. It was observed that the normalized absorption spectrum of ranitidine highly overlapped with the normalized excitation spectrum of **1′** and this did not occur in the cases of other analytes (Fig. S79†). The IFE-based sensing mechanism was further investigated by introducing the IFE correction factor. Here, the quenching efficiency was calculated after removing the contribution of IFE for quenching. The obtained results are depicted in Fig. S81 and Table S6.† After removing the IFE contribution, the considerable drop in quenching efficiency suggested that the IFE is the most probable mechanism for ranitidine sensing. Although IFE was previously considered an error in fluorescence measurements, it is well established now as a non-irradiative mechanistic model for energy transfer in the spectroscopic technique. It has been used to develop various photoluminescence-based sensors.[39,40] From all the above experimental results, we can conclude that the ground state complexation and IFE are the most plausible reasons behind the fluorescence quenching of **1′** in the presence of Hg^{2+} and ranitidine, respectively.

150 | *Inorg. Chem. Front.*, 2024, **11**, 142–155

This journal is © the Partner Organisations 2024

Catalysis of Friedel–Crafts alkylation using 1′

The potential ability of **1′** for heterogeneous catalysis was examined in Friedel–Crafts alkylation between IND and NS as classical substrates. The reaction conditions were optimized. The observed results are discussed below. The Friedel–Crafts alkylation reaction between IND and NS was performed in toluene at 70 °C for 24 h using **1′** as a solid catalyst. Under these experimental conditions, this reaction afforded 98% yield of the anticipated product. Fig. 8 displays the time yield plots for the reaction between IND and NS when **1′** was employed as a catalyst. Under similar conditions, the activity of Al-MIL-53-NH$_2$ was investigated and a significantly lower yield of the targeted product was observed. These data unambiguously suggest that thioureido functionalities embedded within the framework of MOFs significantly contribute to facilitate the reaction. These results agree with earlier reports,[18] suggesting the involvement of hydrogen bond donating sites. Thus, the activity of MOFs has been significantly improved with appropriate functionalization in the linker with amide, urea, thiourea and squaramide moieties. These groups are responsible for activating IND and NS within the confined environment of the MOF. On the other hand, the yield of the product also decreased upon decreasing the reaction temperature and catalyst loading. The reaction between NS and IND using 10 mg of **1′** as a solid catalyst at 50 °C showed 64% yield after 24 h while 5 mg of **1′** provided 55% yield after 24 h.

A mandatory experiment in heterogeneous catalysis is to perform leaching and reusability tests to ascertain catalyst integrity under the optimized conditions. Leaching experiment was conducted under the optimized reaction conditions and the solid was filtered after 1 h. The remaining reaction mixture was continued without the solid catalyst and the reaction rate was compared with the reaction rate in the presence of the solid catalyst. Comparison of the product yields between these two reactions clearly indicates that the reaction did not proceed further after the removal of the solid catalyst. Hence, the reaction occurs *via* a heterogeneous manner without leaching of any active site into solution. The solid catalyst was recovered after the reaction through filtration. After washing and proper drying, it was used again in successive cycles. Fig. 9 shows that **1′** could retain its performance up to four cycles without any decay in its yield. Furthermore, FE-SEM images and PXRD patterns also suggest that the particle morphology and crystallinity of the used solid were not affected with respect to the fresh solid catalyst (Fig. S82 and S83†). Thus, these results imply the stability of **1′** under the present experimental conditions.
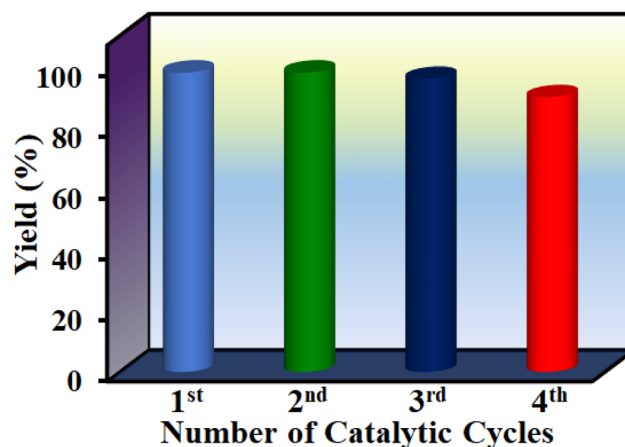

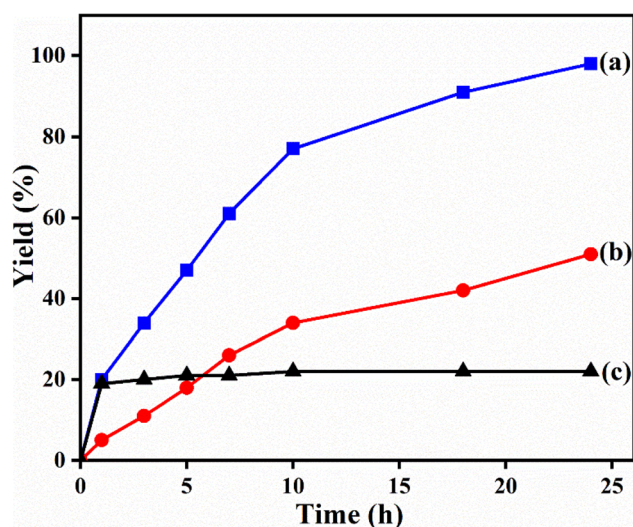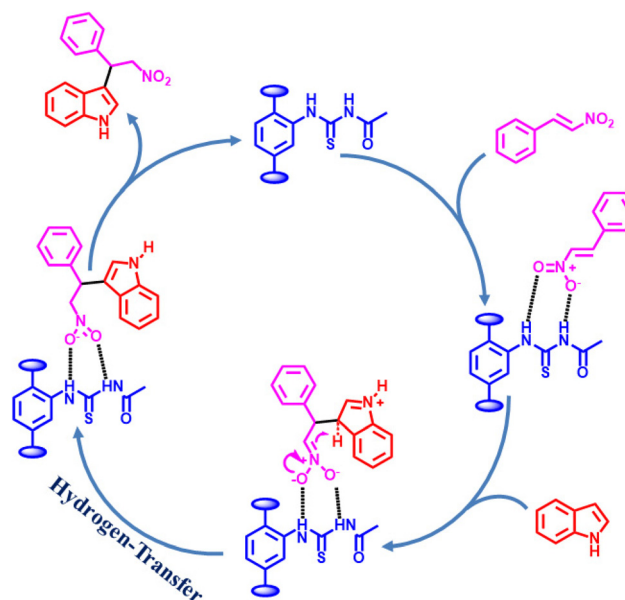**Fig. 9** Reusability experiments for the Friedel–Crafts reaction of NS with IND using **1′**.

Fig. 8 Time–yield plots for Friedel–Crafts alkylation between IND and NS using (a) **1′** as a solid catalyst, (b) MIL-53(Al)-NH$_2$ as a catalyst and (c) leaching test in the absence of **1′**.
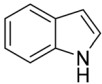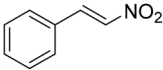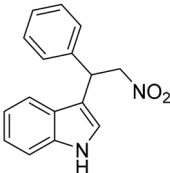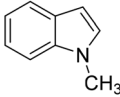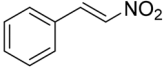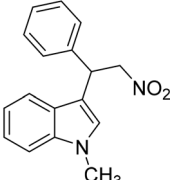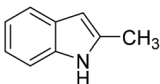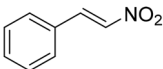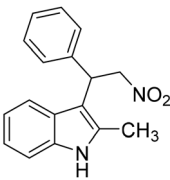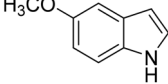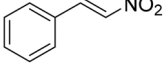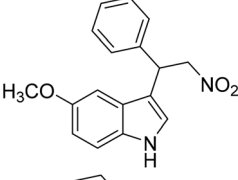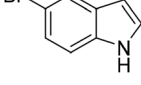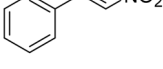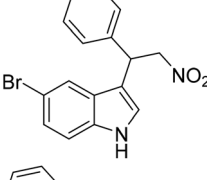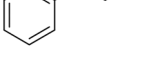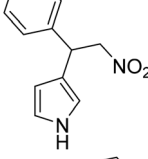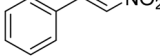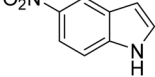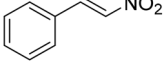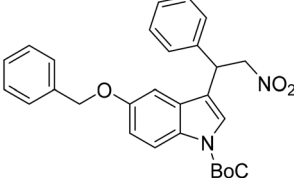

Scheme 2 Proposed mechanism for the Friedel–Crafts alkylation between IND and NS using **1′** as a catalyst.

Considering the activity achieved with **1′** as a catalyst for the Friedel–Crafts alkylation reaction between IND and NS, a possible mechanism is proposed and it is shown in Scheme 2. As can be seen in Scheme 2, the thioureido moieties in **1′** interact with NS by establishing hydrogen bonding. This is one of the important intermediates to alter electron density in NS and

Table 1 Friedel–Crafts alkylation of IND derivatives with NS employing **1′** as a solid catalyst[a]

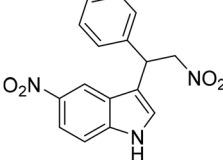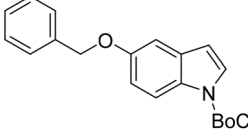| S. no	IND	NS	Product	Yield[b] (%)
1.				98
2.				96
3.				98
4.				97
5.				54
6.				93
7.				—
8.				—

[a] Reaction conditions: IND (0.1 mmol), NS (0.105 mmol), toluene (0.1 mL), 70 °C, **1′** (10 mg), 24 h. [b] Isolated yields are confirmed by ^{1}H-NMR and GC-MS.

152 | *Inorg. Chem. Front.*, 2024, **11**, 142–155

This journal is © the Partner Organisations 2024

such intermediates have been reported in the literature due to the involvement of hydrogen bond donating sites.[41–43] Thus, the activity of **1′** was significantly higher compared to that of MIL-53(Al)-NH$_2$ as a catalyst under similar conditions. This interaction of NS with hydrogen bonding sites creates electron deficiency in the C=C double bond of NS. Furthermore, IND attacks NS through the C3 carbon to afford the desired product. Thus, the catalyst can be regenerated and recycled in subsequent cycles.

The catalytic activity of **1′** with different substrates as well as the size-selective catalytic behaviour was investigated (Table 1 and Fig. S84–S95†). The above optimized conditions were considered to prepare a series of heterocyclic compounds. In this aspect, the reaction of IND with NS afforded 98% yield utilizing **1′** at 70 °C in toluene after 24 h. Under identical conditions, the reaction of 1-methylindole and NS resulted in 96% yield using **1′** as a solid catalyst. A similar activity was also observed for the reaction between 2-methylindole and NS with **1′** as a catalyst under identical conditions. The reaction of 5-methoxyindole and 5-bromoindole with NS gave 97 and 54% yields using **1′** as a catalyst under the same conditions. The coupling between pyrrole and NS was also efficient to achieve 93% yield using **1′** as a catalyst. Under the same conditions, no product was obtained when 5-nitroindole was reacted with NS. Furthermore, efforts to perform the reaction between *N*-Boc protected IND and NS using **1′** as a solid catalyst also failed. This is a suitable example to illustrate size selective catalysis. It suggests that the diffusion of the larger substrates towards the active sites is hindered due to their larger kinetic dimensions and thus no reaction occurred.

Conclusion

In this work, a novel thioureido functionalized aluminium MOF was applied for selective and rapid sensing of a heavy metal ion (Hg^{2+}) and an anti-histamine drug (ranitidine) in aqueous and HEPES media, respectively. The designed probe is the first MOF for recognition of ranitidine. The sensor showed a fast response time with 93% fluorescence quenching within 10 s for Hg^{2+} and 98% within 5 s for ranitidine. The detection limits for Hg^{2+} and ranitidine were determined to be 7.3 nM and 3.4 nM, respectively, which are lower or comparable to those of the existing fluorescent sensors. We explored the sensing ability in various biological media (serum and urine), various water specimens, and even in pH media. Furthermore, the MOF detected ranitidine in pharmaceutical samples, highlighting its potential for practical applications. To enhance the practical utility of the MOF, we developed a **1′**@PVDF-PVP composite membrane, which exhibited fluorescence quenching upon exposure to Hg^{2+} and ranitidine. The composite showed potential for real-field sensing applications, providing a more stable and reusable platform than other reported composites. The mechanism of fluorescence quenching was investigated, and it was found that ground-state complexation and the inner filter effect were the most

probable reasons behind the fluorescence quenching of **1′** upon addition of Hg^{2+} and ranitidine, respectively. We believe this work will contribute to advancing efficient and practical fluorescent probes for environmental and biomedical applications. Furthermore, the catalytic activity of **1′** was convincingly demonstrated in the Friedel–Crafts alkylation reaction between IND and NS in 98% yield at 70 °C. The absence of leaching was confirmed by the hot-filtration experiment. The catalyst was efficiently reused up to four cycles. Owing to its broad substrate scope, the catalyst can be utilized to obtain a series of heterocyclic compounds.

Author contributions

All the experiments were carried out by SSH and VK. Scientific advices were obtained from SB and AD.

Conflicts of interest

There are no conflicts to declare.

Acknowledgements

References

1 S. Cai, K. Lao, C. Lau and J. Lu, "Turn-on" chemiluminescence sensor for the highly selective and ultrasensitive detection of Hg2+ions based on interstrand cooperative coordination and catalytic formation of gold nanoparticles, *Anal. Chem.*, 2011, **83**, 9702–9708.

2 S. Ekino, M. Susa, T. Ninomiya, K. Imamura and T. Kitamura, Minamata disease revisited: an update on the acute and chronic manifestations of methyl mercury poisoning, *J. Neurol. Sci.*, 2007, **262**, 131–144.

3 A. Carocci, N. Rovito, M. S. Sinicropi and G. Genchi, Mercury toxicity and neurodegenerative effects, *Rev. Environ. Contam. Toxicol.*, 2014, 1–18.

4 M. Bogush, N. A. Heldt and Y. Persidsky, Blood brain barrier injury in diabetes: unrecognized effects on brain and cognition, *J. NeuroImmune Pharmacol.*, 2017, **12**, 593–601.

5 N. Rutledge, *Engineering chemistry, Scientific e-Resources*, 2018.

This journal is © the Partner Organisations 2024

Inorg. Chem. Front., 2024, **11**, 142–155 | **153**

6 J. Mills, K. Koch, C. Webster, M. Sirgo, K. Fitzgerald and J. Wood, The safety of ranitidine in over a decade of use, *Aliment. Pharmacol. Ther.*, 1997, **11**, 129–137.

7 T. Vial, C. Goubier, A. Bergeret, F. Cabrera, J.-C. Evreux and J. Descotes, Side effects of ranitidine, *Drug Saf.*, 1991, **6**, 94–117.

8 M. B. Evans, P. A. Haywood, D. Johnson, M. Martin-Smith, G. Munro and J. C. Wahlich, Chromatographic methods for determining the identity, strength and purity of ranitidine hydrochloride both in the drug substance and its dosage from—an exercise in method selection, development, definition and validation, *J. Pharm. Biomed. Anal.*, 1989, **7**, 1–22.

9 A. L. Suherman, S. Kuss, E. E. Tanner, N. P. Young and R. G. Compton, Electrochemical Hg 2+detection at tannic acid-gold nanoparticle modified electrodes by square wave voltammetry, *Analyst*, 2018, **143**, 2035–2041.

10 S. Mukherjee, S. Ghosh and S. Biswas, A MOF chemosensor for highly sensitive and ultrafast detection of folic acid in biofriendly medium, paper strips and real samples, *Inorg. Chem. Front.*, 2022, **9**, 6288–6298.

11 G. He, Y. Zhao, C. He, Y. Liu and C. Duan, "Turn-on" fluorescent sensor for Hg2+via displacement approach, *Inorg. Chem.*, 2008, **47**, 5169–5176.

12 D. Huang, C. Niu, X. Wang, X. Lv and G. Zeng, "Turn-on" fluorescent sensor for Hg2+based on single-stranded DNA functionalized Mn: CdS/ZnS quantum dots and gold nanoparticles by time-gated mode, *Anal. Chem.*, 2013, **85**, 1164–1170.

13 L. Zhang, T. Li, B. Li, J. Li and E. Wang, Carbon nanotube–DNA hybrid fluorescent sensor for sensitive and selective detection of mercury(II) ion, *Chem. commun.*, 2010, **46**, 1476–1478.

14 S. Ghosh, F. Steinke, A. Rana and S. Biswas, A fluorescent zirconium organic framework displaying rapid and nanomolar level detection of Hg (ii) and nitroantibiotics, *Inorg. Chem. Front.*, 2022, **9**, 859–869.

15 L. E. Kreno, K. Leong, O. K. Farha, M. Allendorf, R. P. Van Duyne and J. T. Hupp, Metal–organic framework materials as chemical sensors, *Chem. Rev.*, 2012, **112**, 1105–1125.

16 H.-Y. Li, S.-N. Zhao, S.-Q. Zang and J. Li, Functional metal–organic frameworks as effective sensors of gases and volatile compounds, *Chem. Soc. Rev.*, 2020, **49**, 6364–6401.

17 A. Dhakshinamoorthy, A. M. Asiri and H. Garcia, Metal–organic frameworks as multifunctional solid catalysts, *Trends Chem.*, 2020, **2**, 454–466.

18 A. Dhakshinamoorthy, A. M. Asiri and H. García, New Opportunities in Metal Organic Framework Catalysis: From Bifunctional to Frustrated Lewis Pairs Catalysis, *Chem. – Eur. J.*, 2023, e202204016.

19 N. T. Phan, K. K. Le and T. D. Phan, MOF-5 as an efficient heterogeneous catalyst for Friedel–Crafts alkylation reactions, *Appl. Catal., A*, 2010, **382**, 246–253.

20 E. Rahmani and M. Rahmani, Al-based MIL-53 metal organic framework (MOF) as the new catalyst for Friedel–Crafts alkylation of benzene, *Ind. Eng. Chem. Res.*, 2018, **57**, 169–178.

21 A. Dhakshinamoorthy, A. M. Asiri and H. Garcia, Catalysis in confined spaces of metal organic frameworks, *ChemCatChem*, 2020, **12**, 4732–4753.

22 M. Singh and S. Neogi, Largely Entangled Diamondoid Framework with High-Density Urea and Divergent Metal Nodes for Selective Scavenging of CO2 and Molecular Dimension-Mediated Size-Exclusive H-Bond Donor Catalysis, *Inorg. Chem.*, 2022, **62**, 871–884.

23 J. Q. Wu, X. Y. Wu, J. M. Lu, Q. Shi and L. X. Shao, Highly Active La(III)–Based Metal–Organic Framework as a Heterogeneous Lewis Acid Catalyst for Friedel–Crafts Alkylation, *Chem. – Eur. J.*, 2022, **28**, e202202441.

24 M. Singh, P. P. Mondal, S. Rajput and S. Neogi, Contrasting-functionality-decked robust MOF for moisture-tolerant and variable-temperature CO 2 adsorption with in-built urea group mediated mild condition cycloaddition, *Inorg. Chem. Front.*, 2023, **10**, 3605–3620.

25 A. Das, N. Anbu, M. Sk, A. Dhakshinamoorthy and S. Biswas, Highly active urea-functionalized Zr(IV)-UiO-67 metal–organic framework as hydrogen bonding heterogeneous catalyst for Friedel–Crafts Alkylation, *Inorg. Chem.*, 2019, **58**, 5163–5172.

26 N. Nagarjun, P. Concepcion and A. Dhakshinamoorthy, Influence of oxophilic behavior of UiO–66 (Ce) metal–organic framework with superior catalytic performance in Friedel–Crafts alkylation reaction, *Appl. Organomet. Chem.*, 2020, **34**, e5578.

27 D. Markad and S. K. Mandal, Design of a primary-amide-functionalized highly efficient and recyclable hydrogen-bond-donating heterogeneous catalyst for the Friedel–Crafts alkylation of indoles with β-nitrostyrenes, *ACS Catal.*, 2019, **9**, 3165–3173.

28 A. Nagaraj and D. Amarajothi, Cu3 (BTC) 2 as a viable heterogeneous solid catalyst for Friedel-Crafts alkylation of indoles with nitroalkenes, *J. Colloid Interface Sci.*, 2017, **494**, 282–289.

29 C. M. McGuirk, M. J. Katz, C. L. Stern, A. A. Sarjeant, J. T. Hupp, O. K. Farha and C. A. Mirkin, Turning on catalysis: incorporation of a hydrogen-bond-donating squaramide moiety into a Zr metal–organic framework, *J. Am. Chem. Soc.*, 2015, **137**, 919–925.

30 X. Wang, K. Batra, G. Clavier, G. Maurin, B. Ding, A. Tissot and C. Serre, Ln–MOF Based Ratiometric Luminescent Sensor for the Detection of Potential COVID–19 Drugs, *Chem. – Eur. J.*, 2023, **29**, e202203136.

31 T. Loiseau, C. Serre, C. Huguenard, G. Fink, F. Taulelle, M. Henry, T. Bataille and G. Férey, A rationale for the large breathing of the porous aluminum terephthalate (MIL–53) upon hydration, *Chem. – Eur. J.*, 2004, **10**, 1373–1382.

32 S. Neogi, M. K. Sharma and P. K. Bharadwaj, Knoevenagel condensation and cyanosilylation reactions catalyzed by a MOF containing coordinatively unsaturated Zn(II) centers, *J. Mol. Catal. A: Chem.*, 2009, **299**, 1–4.

33 Y. Zhao, H. Wu, T. J. Emge, Q. Gong, N. Nijem, Y. J. Chabal, L. Kong, D. C. Langreth, H. Liu and H. Zeng, Enhancing gas adsorption and separation capacity through

154 | *Inorg. Chem. Front.*, 2024, **11**, 142–155

This journal is © the Partner Organisations 2024

ligand functionalization of microporous metal–organic framework structures, *Chem. – Eur. J.*, 2011, **17**, 5101–5109.

34 A. Rana, C. Gogoi, S. Ghosh, S. Nandi, S. Kumar, U. Manna and S. Biswas, Rapid recognition of fatal cyanide in water in a wide pH range by a trifluoroacetamido based metal–organic framework, *New J. Chem.*, 2021, **45**, 20193–20200.

35 F. Hekmat, M. A. Kachouei, S. T. Foshtomi, S. Shahrokhian and Z. Zhu, Direct decoration of commercial cotton fabrics by binary nickel-cobalt metal-organic frameworks for flexible glucose sensing in next-generation wearable sensors, *Talanta*, 2023, **257**, 124375.

36 P. Chakraborty, A. Rana, S. Mukherjee and S. Biswas, Metal–Organic-Framework-Based Chemosensor for Ultrafast and Ultrasensitive Detection of Pd2+ Ions in Water, Real Specimens, and Test Strips, *Inorg. Chem.*, 2022, **62**, 802–809.

37 A. Rana and S. Biswas, Electrophilicity modulated targeted luminescence of MOF-coated cotton composite for dual analyte detection in aqueous medium, *Inorg. Chem. Front.*, 2023, **10**, 2742–2753.

38 N. Alam, S. Mondal, S. S. Hossain, S. Sahoo and D. Sarma, Lanthanide-Directed Luminescent "Soft" Coordination Polymer Gels: White Light Emission, Anticounterfeiting, and Thin-Film-Based Sensing, *ACS Appl. Eng. Mater.*, 2023, **1**, 1201–1212.

39 S. Ghosh, J. Krishnan, S. S. Hossain, A. Dhakshinamoorthy and S. Biswas, MOF-Fabric Composites Based on a Multi-Functional MOF as Luminescent Sensors for a Neurotransmitter and an Anti-Cancer Drug, *ACS Appl. Mater. Interfaces*, 2023, **15**, 26843–26851.

40 P. Sarkar, M. Saha, N. Nandi, D. K. Sahu and K. Sahu, Red-Emitting Silver Nanoclusters for Dual-Mode Detection of Cu2+ and Vitamin B12 in Living Cells, *ACS Appl. Nano Mater.*, 2022, **5**, 7670–7678.

41 G. Dessole, R. P. Herrera and A. Ricci, H-bonding organocatalysed Friedel-Crafts alkylation of aromatic and heteroaromatic systems with nitroolefins, *Synlett*, 2004, 2374–2378.

42 J. M. Roberts, B. M. Fini, A. A. Sarjeant, O. K. Farha, J. T. Hupp and K. A. Scheidt, Urea metal–organic frameworks as effective and size-selective hydrogen-bond catalysts, *J. Am. Chem. Soc.*, 2012, **134**, 3334–3337.

43 E. Fan, S. A. Van Arman, S. Kincaid and A. D. Hamilton, Molecular recognition: hydrogen-bonding receptors that function in highly competitive solvents, *J. Am. Chem. Soc.*, 1993, **115**, 369–370.

This journal is © the Partner Organisations 2024

Inorg. Chem. Front., 2024, **11**, 142–155 | **155**